Carbon 169 (2020) 482–487

Contents lists available at ScienceDirect

Carbon

journal homepage: www.elsevier.com/locate/carbon

Focused ion beam deposited carbon-platinum nanowires for cryogenic resistive thermometry

Kirsten Blagg [a, *], Portia Allen [a], Tzu-Ming Lu [b], Michael P. Lilly [b], Meenakshi Singh [a]

[a] Colorado School of Mines, Golden, CO, 80401, USA
[b] Center for Integrated Nanotechnologies, Sandia National Laboratories, Albuquerque, NM, USA, 87123

ARTICLE INFO

Article history:
Received 26 May 2020
Received in revised form
24 June 2020
Accepted 29 June 2020
Available online 4 August 2020

Keywords:
Focused ion beam
Carbon-platinum
Nanowire
Low temperature thermometry
Cryogenic

ABSTRACT

The study of thermal effects, both classical and quantum, at cryogenic temperatures requires the use of on-chip, local, high-sensitivity thermometry. Carbon-platinum composites fabricated using focused ion beam (FIB) assisted deposition form a granular structure which is shown in this study to be uniquely suited for this application. Carbon-platinum thermometers deposited using a 24 pA ion beam current have high sensitivities below 1 K, comparable to the best cryogenic thermometers. In addition, these thermometers can be accurately placed to within 10s of nanometers on the chip using a mask-free process. They also have a weak magnetic field dependence, < 3% change in resistance with applied magnetic fields from 0 to 8 T. Finally, these thermometers are integrable into a variety of nanoscale devices due to the existing wide spread use of FIB.

1. Introduction

Measuring thermal effects at cryogenic temperatures is the gateway to a large number of relatively uncharted domains such as quantum thermodynamics [1], quantum thermoelectric effects [2,3], quantized heat flows [4], the thermal Josephson effect [5], and quantum heat engines [6,7]. These studies often require the use of nanoscale thermometers with high sensitivity at cryogenic temperatures which can be patterned directly onto a device. Historically, a variety of techniques have been used for this including measurements of noise, tunneling current, resistance, and capacitance. Of these techniques, resistive thermometry is particularly popular due to accessible fabrication and the ease of low noise measurements. Materials such as RuO_2 [8,9], CrN [10], ZrN [11], GeGaAs [12,13], NbN [14–16], NiCr [17], InSb [18], and TiPt [19] have been used as resistive cryogenic thermometers (Table 1). However, nanoscale, on-chip fabrication of these thermometers requires the use of electron beam lithography (EBL) and stoichiometric deposition. EBL, which allows for precise micro and nano fabrication, requires the use of a resist that may cause contamination or destroy delicate suspended platforms. To our knowledge, there exists no mask-less local thermometery techniques for cryogenic temperatures. In this paper, we examine the use of focused ion beam deposited carbon-platinum (FIB C-Pt) composite as a sensitive, local, microthermometer at cryogenic temperatures which can be deposited without the use of a mask at any stage of device fabrication.

FIB deposition is a commonly used method to obtain nanoscale, ohmic contacts [20]. As a result, it has been studied extensively in this role. In particular, the resistivity of FIB C-Pt has been studied with respect to composition [21–23], temperature [24–27], size [28,29], and deposition parameters [30,31]. However, the potential of FIB C-Pt as a cryogenic, resistive thermometer has never been studied. While, the composite system represents a novel method of on-chip thermometry, its components, elemental Pt [32–37] and C [32,38,39], have been utilized as resistive thermometers for a variety of applications. For pure Pt thermometers, as with most metallic thermometers, the temperature dependence of resistivity is due to changes in electron-phonon scattering. This saturates below 10 K for Pt [32] causing a loss of sensitivity. Alternatively, commercial carbon resistors (Allen–Bradley, Matsushita, Speer) have high sensitivity at cryogenic temperatures. The R-T characteristics of these thermometers is based on the carbon particulates creating an impure, irregular composite. However, carbon thermometry, which utilizes macroscale carbon resistors, is inadequate for local microscale measurements. FIB C-Pt utilizes a simple, high-

* Corresponding author.
E-mail address: kblagg@mines.edu (K. Blagg).

https://doi.org/10.1016/j.carbon.2020.06.087
0008-6223/

Table 1
Compilation of thin film resistive thermometers used for cryogenic applications including: thermometer material, applicable temperature range, range of sensitivity in the applicable temperature range given by $S = \frac{T}{V}\frac{dV}{dT} = \frac{d(\log V)}{d(\log T)}$, and maximum magnetic field induced variation in the applicable temperature range up to 8 T given as the temperature shift due to the magnetic field ($\Delta T = \Delta R/R_{0T}{}^{*}T/S$). Results of the present work are given for FIB C-Pt thermometers deposited at 24 pA.

Material	Temperature Range (K)	Sensitivity	Magnetic field induced variation (K)
RuO_2 [8,9]	0.01–1.6	0.25–2.8	0.004–0.02
CrN [10]	1.8–300	1–2	0.04–0.05
ZrN [11]	2–300	0.14–0.54	0.045–0.09
Ge-GaAs [12,13]	0.03–500	0.1–4.3	0.30–23.31
NbN [16]	0.10–300	0.7–3.7	0.04–0.30
NiCr [17]	0.4–4	0.1–4.7	_
InSb [18]	0.01–10	0.1–100	0–2
FIB C-Pt (this work)	0.1–8	0.001–14.88	0.04

resolution deposition method to form a granular composite material of 3–8 nm platinum inclusions embedded in an amorphous carbon matrix [21,22,25,30]. The C-Pt composite leads to complex conduction characteristics at low temperatures that are independent of either carbon or platinum. In this study, C-Pt composite thermometers are deposited using different ion beam currents. Differences in deposition current lead to changes in composition and morphology that determine the sensitivity of the composite. In particular, thermometers deposited with a 24 pA ion current show sensitivity comparable to RuO_2 and Cernox, two leading commercially available resistive thermometery technologies, over a wide temperature range (Table 1).

2. Methods

FIB C-Pt thermometers were deposited on an RCA cleaned Si substrate with a thermally grown 240 nm SiO_2 layer using an FEI Helios Nanolab 600i. The C-Pt precursor gas, $(CH_3)_3(CH_3C_5H_4)Pt$, was heated to 45–46 °C. Each wire was deposited via a 290–300 pC/μm dose, 30 kV ion voltage, 200 ns dwell time, 150% overlap, and a current between 6.5 pA and 226.5 pA. Each thermometer is 10 μm in length, 100 nm in width, and 150 nm in height (Fig. 1). Structural characterization using transmission electron microscopy (TEM) and energy dispersive x-ray spectroscopy (EDS) was performed. Electrical contact to the thermometer was made using a combination of FIB leads and photolithographically patterned thermally evaporated aluminum contact pads. The sample was connected to the chip carrier via gold wire bonding.

The sample was then cooled down in a helium 3 (He3) or dilution refrigerator (DR). The resistance of the sample as a function of fridge temperature, monitored using a RuO_2 thermometer thermally anchored to the He3 pot (He3) or mixing chamber (DR), was measured using standard lock-in techniques with an excitation current of 100 nA. This excitation current corresponds to a power of ~ 0.01 nW where heating effects are negligible. It was determined in separate measurements that heating effects become important at a power of ~ 1 nW in our set up.

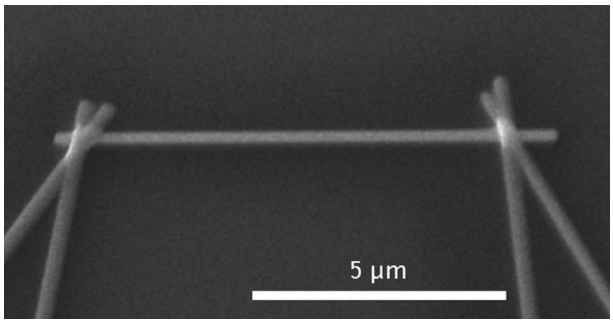

Fig. 1. Field emission scanning electron microscope (FESEM) image of focused ion beam (FIB) deposited C-Pt wire with four probe electrical contacts deposited via FIB C-Pt.

3. Composition and structural characterization

In FIB assisted deposition, the interaction of a focused ion beam (typically Ga) with the substrate and a precursor gas causes the deposition of desired material. This process is influenced by numerous parameters including: interaction volume of the beam with the substrate, mass and penetration depth of ions, energy and mean free path of the generated electrons, ion implantation, thermal diffusion, residual pressure, gas flux, beam overlap, dwell time, ion dose, and focus. Since varying deposition parameters for the thermometers changes their composition and morphology, structural characterization of the thermometers is critical.

A field emission scanning electron microscope (FESEM, JEOL 7000) was used to image the thermometers and to perform EDS to determine the composition of each nanowire. In order to increase the signal for EDS, calibration wires 10 μm in length, 1 μm in width, and 150 nm thick were deposited on an Si/SiO_2 substrate. Each sample was measured using a 30 kV electron beam with a spot size of approximately 1 μm. Due to the large spot size, the EDS raw spectra includes both the thermometer and the substrate (Fig. 2a). As oxygen contamination in the FIB sample is expected to have a negligibly small signature [21,23], the silicon and silicon dioxide of the substrate are responsible for the silicon and oxygen signal in the EDS spectra. To determine the chemical composition of each wire, these were subtracted from the data and the data was re-normalized to include only the carbon, gallium, and platinum peaks. The chemical composition of the thermometers was measured as a function of ion beam current (Fig. 2b). For each deposition current the wire is mostly carbon. Carbon content decreases from 70–80% at low deposition currents to 50–60% at the highest deposition current. The remaining composition of the wire is divided between Pt and Ga. For all deposition currents the Ga contamination is less than Pt. A small local maximum of Pt content appears at 24 pA deposition current. The composition varied an average of 3.1% between samples and 1% within a sample (Fig. 2b).

For TEM imaging, thermometers 10 μm in length, 100 nm in width, and 150 nm in height were deposited directly on a carbon mesh grid (Ted Pella) using a 8 pA, 24 pA, and 42 pA ion-beam current. FIB deposition on to a carbon grid has been found to be comparable to deposition on SiO_2 [30]. The TEM image, acquired in a FEI Talos F200X, of a thermometer deposited at 24 pA (Fig. 3a) shows Pt nanoparticles embedded in a C matrix. Each grain was measured in three different directions in an image processing software and the measurements were averaged to account for any granular asymmetry. To get a composite average, this measurement

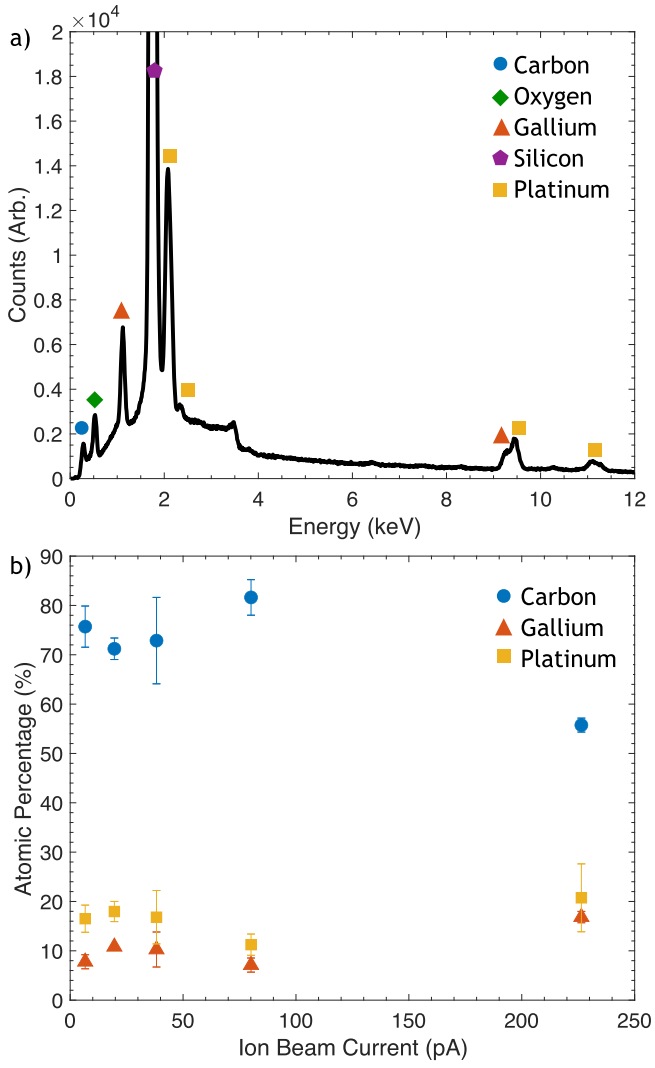

Fig. 2. a) Energy dispersive spectroscopy data from a wire deposited with a 24 pA ion beam current on an Si/SiO_2 substrate. Silicon and oxygen peaks from the substrate are indicated by the purple hexagon and green diamond respectively. The remaining peaks indicate the FIB deposited wires contain platinum (yellow square), carbon (blue circle), and gallium (red triangle). b) Composition of the FIB deposited wires is shown as cumulative atomic percentage from the EDS spectra of three wires at each deposition current. The data is normalized to exclude the substrate (Si and O). Carbon is indicated by blue circles, platinum by yellow squares, and gallium by red triangles. (A colour version of this figure can be viewed online.)

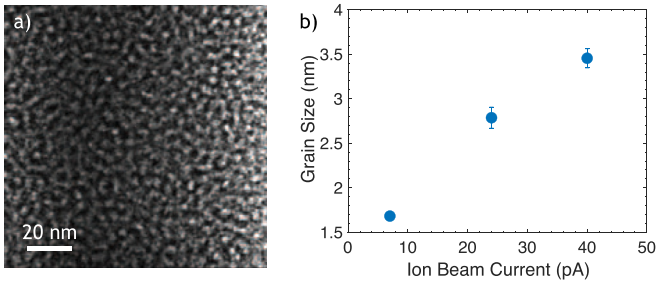

Fig. 3. a) A TEM image of FIB C-Pt deposited at 24 pA ion current. The dark spots indicate the granular Pt embedded in a carbon matrix (light background). b) Ion beam deposition current versus grain size as measured by TEM. The grain size increases with increasing ion current. (A colour version of this figure can be viewed online.)

was completed on 84–92 grains for each wire. As the ion beam current of the FIB increases, the grain size of the Pt nanoparticles also increases (Fig. 3b).

4. Electronic transport characterizations

Room temperature resistivity of the thermometers was measured as a function of ion beam deposition current using a standard four probe configuration with ohmic contacts (Fig. 4). This measurement was performed on five samples deposited at each ion current immediately after deposition. The systematic change in resistivity as a function of ion beam current seen in Fig. 4 is attributable to the change in composition and grain size of the samples with beam current. Fig. 4 inset shows a linear decrease in room temperature resistivity versus grain size. This dependence is probably due to the increased scattering of electrons at grain boundaries as the number of grains boundaries per unit length increases.

The variance in resistivity between samples of a particular current is typical of disordered granular structures. As resistivity is dependent on electrons scattering off grain boundaries and coupling irregularities, conduction is highly dependent on the disorder of the system and thus variable between samples [40]. The small variability in composition and morphology (1–3%) for a fixed ion beam current leads to a much larger variability in the room temperature resistance (up to 46% at 8 pA). At room temperature, the change is within an order of magnitude. However, at low temperature the difference in resistivity between samples deposited at different currents grows to up to three orders of magnitude. This sensitivity is predicted for granular composites which have a composition near the percolation threshold, about 36% conductive material [41] and has been seen in previous studies of FIB C-Pt [24].

The resistivity measurement on two samples at each deposition current was repeated at regular intervals for a period of 60 days to assess the stability of the thermometer in atmosphere. The samples exhibited a range of increase in resistivity (0.3%–35%) due to oxidation. In all samples the resistivity increased for the first three

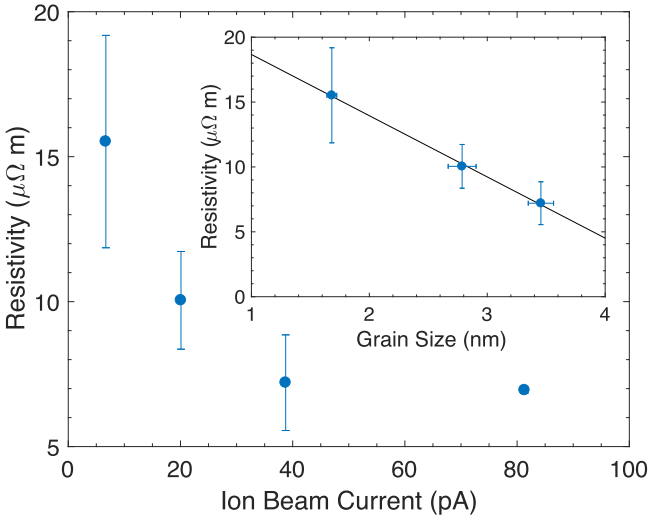

Fig. 4. Room temperature resistivity of FIB C-Pt wires as a function of ion deposition current measured using a standard four probe technique. The resistivity decreases with increasing ion current in a measured range 8 pA–220 pA. The variability between samples as indicated by the error bars also decreases with increasing ion current. Inset: Room temperature resistivity decreases linearly as a function of grain size. (A colour version of this figure can be viewed online.)

to five days and then became constant. This demonstrates that the thermometers have a self-limiting oxidation time of approximately five days and are stable in atmosphere. Other metallic nanoparticles show similar oxidation patterns when embedded in insulating matrices, where oxidation varies with the distribution of the metallic nanoparticles [42,43]. Although bulk platinum is robust against oxidation, Pt nanoparticles have been known to oxidize [44].

Low temperature resistivity measurements were performed from 10 mK to 10 K in a 0–8 T magnetic field. The nanowires are ohmic at the excitation currents used. The resistivity as a function of temperature (Fig. 5) shows evidence of multiple conduction mechanisms commonly found in metallic granular structures [40]. In previous studies of FIB C-Pt, electronic transport has been attributed to variable range hopping [22,26,30,45], a percolation conduction model [24], metallic conduction [25,28], and metal to insulator transitions [21]. Here we observe three regions in the resistance vs. temperature behavior in the temperature range relevant to cryogenic applications (Fig. 5a inset). Region I, the highest temperature region, is one in which the wire acts as a highly resistive metal and conductivity is primarily defined by electron-phonon scattering. Since most phonons are frozen at these temperatures ($\sim$ 10 K), resistance shows a weak dependence on temperature ($dR/dT \sim 0$) [46]. This flattening of dR/dT has been seen before in C-Pt composites and explained using the Bloch-Gruneisen formalism with a reduced Debye temperature [28]. As the sample continues to cool, we arrive at region II, or the medium temperature regime (0.6–6 K in the inset of Fig. 5). In this regime, the resistance decreases rapidly with decreasing temperature for all except the most metallic samples. The large $dR/dT > 0$ in region II, typically only seen at much higher temperatures, has not been observed in this system before. The physical mechanism governing this dependence is currently not well understood. At the lowest temperatures, defined as region III (< 0.6 K in the inset of Fig. 5), the R(T) depends sensitively on sample morphology. The most metallic samples remain saturated (similar to regions I and II). The most disordered samples tend to undergo a metal to insulator transition [21]. The intermediate samples continue to display positive dR/dT in region III. The C-Pt thermometers which show this positive R(T) dependence in regions II and III are shown below to be sensitive, reproducible thermometers.

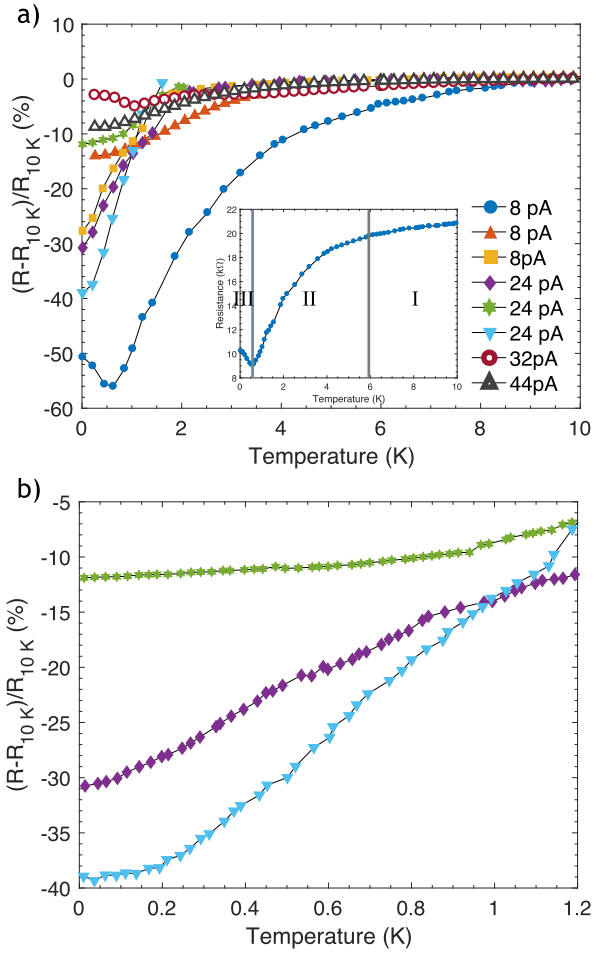

Fig. 5. a) Percent change in resistance ($R - R_{10K}/R_{10K}$) of C-Pt deposited at different ion currents measured as a function of temperature. The resistance at 10 K ranges in value from 0.2 to 14 kΩ. The resistivity characterizations vary between deposition parameters and sample. Inset: Resistance of a FIB C-Pt thermometer deposited at 8 pA as a function of temperature. Conduction is divided into three regions with distinct conduction mechanisms. The boundary between regions is indicative of a qualitative change in transport behavior and is not meant to represent a sharp transition. b) Ultra low temperature resistance of three FIB C-Pt thermometers deposited at 24 pA measured as a function of temperature. (A colour version of this figure can be viewed online.)

The samples deposited at higher currents (32 pA and 44 pA, Fig. 5a) have the largest metallic grain sizes (see Fig. 4 inset) and behave like high resistivity metals in regions I and II. Akin to the saturation of metallic resistivity at these temperatures due to the freezing of phonon modes, the resistivity in these samples is not a rapidly changing function of temperature. In regions I and II, the metallic type thermometers have an average sensitivity ($-d(\log V)/d(\log T)$) of 0.3 (0.10) and 0.1 (0.05) respectively for the 32 pA (44 pA) thermometer. This makes them relatively poor thermometers in the 1–10 K temperature range. In region III, both metallic thermometers show a tendency to switch to a decreasing temperature dependence ($dR/dT > 0$) and metal insulator transition to different extents ($dR/dT < 0$). But, since they are poor thermometers in most of the temperature range of interest, we did not attempt to optimize them in this small temperature range where they might be acceptable thermometers.

The samples deposited at the lowest current (8 pA) have high variability from sample to sample. Although still qualitatively following the trend of saturation to large positive dR/dT to insulator transition with decreasing temperature, the transition points for a particular sample are largely unpredictable. This is as expected from the wide range of room temperature resistivities (Fig. 4) of these samples which we attribute to unstable deposition rates at low currents. Although some 8 pA samples would make excellent thermometers after calibration, due to their lack of sample to sample reproducibility, we do not propose these as viable thermometers for widespread use.

The 24 pA thermometers fall in the ideal deposition current range where they are neither highly metallic like the 44 pA samples, nor unpredictable like the 8 pA samples. The three samples measured behave qualitatively identically in all three regions, even though the actual values of resistivity and dR/dT vary between samples. In region I, with a relatively large thermal energy present to make tunneling between metallic grains viable, the wires show metallic saturation behavior and are not good cryogenic thermometers. In region II however, they show a large, positive dR/dT with an average sensitivity of 0.8 for the three 24 pA thermometers in this region. This sensitivity compares favorably to RuO_2 thermometers which have an average sensitivity of 0.33 [8] and Cernox

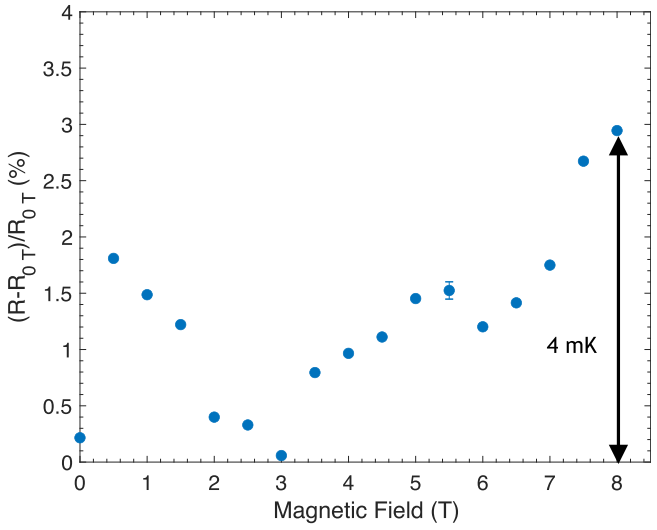

Fig. 6. Percent change in resistance $(R - R_{0T}/R_{0T})$ measured as a function of magnetic field from 0 T to 8 T for a C-Pt wire deposited at 24 pA. The 3% change in resistance corresponds to a 4 mK temperature shift at 10 mK. (A colour version of this figure can be viewed online.)

thermometers which have a sensitivity of 0.61[1] in this region. For the 24 pA samples, the strong R(T) dependence continues into ultra low temperatures in region III (Fig. 5 b). The average sensitivity of the three samples in the figure is 0.1357, 0.3974, and 0.53. At the lowest temperatures, the 24 pA samples do show some tendency towards flattening of the R vs. T curve (light blue triangles in Fig. 5b). Even with reduction in the slope, the sensitivity remains reasonable (0.015). Where the nominal sensitivity is minimum (0.001 in Table 1), the thermometers are still effective and can resolve 5 mK temperature differences due to the low noise of the measurements and the high resistance of the samples. Since the thermometers show quantitative variability between samples, each thermometer requires individual calibration which is standard practice for cryogenic thermometers. The 24 pA thermometers have, on average, a high sensitivity and reproducibility in a wide temperature range from 10 mK to 8 K.

We also characterized the magnetic field dependence of the 24 pA thermometers. Since many low temperature thermal measurements require the use of a magnetic field, the magnetoresistance of the thermometer can lead to a loss of accuracy. Fig. 6 shows the magnetoresistance of a 24 pA thermometer. The magnetoresistance at 10 mK is oscillatory with a maximum percent change in resistance of 3.03% at a field of 8 T. This corresponds to a temperature increase of about 4 mK. Therefore, for the most accurate measurements at lowest temperatures additional calibration in the presence of a magnetic field is required. Since the magnetoresistance was not found to depend strongly on temperature, the temperature variation in a magnetic field reported here is expected to apply for other temperatures as well. This magnetoresistance behavior is comparable to current thin film thermometers (Table 1).

5. Conclusion

Electrical transport in FIB deposited C-Pt composites is highly dependent on deposition parameters. Careful determination of how sample morphology depends on deposition parameters and dictates transport properties has enabled us to obtain optimized deposition parameters for a promising cryogenic, on-chip thermometer. C-Pt composite wires deposited at a low, but stable ion beam current (24 pA) are excellent thermometers in the 10 mK–1.2 K range with on average high sensitivity and small magnetic field dependence comparable to the most widely used cryogenic thermometers (RuO_2). Their performance also remains competitive in the 1.2 K–8 K range. In addition to this wide range of sensitivity and stability, they have the unique advantage of being able to be placed on a chip with 10s of nm precision in a mask less process. These thermometers essentially possess all the advantages of carbon for cryogenic thermometry with the additional ability to be deposited in nanostructures on-chip. Since FIB deposited nanostructures are currently used as electrical probes and can also be used as on-chip joule heaters, these thermometers are amenable for integration with complex devices. The range of unique properties make this C-Pt composite a versatile thermometer for use in myriad classical and quantum thermal measurements.

CRediT authorship contribution statement

Kirsten Blagg: Conceptualization, Methodology, Investigation, Writing - original draft, Visualization. **Portia Allen:** Investigation, Writing - original draft. **Tzu-Ming Lu:** Resources, Writing - review & editing. **Michael P. Lilly:** Resources, Writing - review & editing. **Meenakshi Singh:** Conceptualization, Methodology, Investigation, Writing - original draft, Supervision, Funding acquisition.

Declaration of competing interest

The authors declare the following financial interests/personal relationships which may be considered as potential competing interests: A patent for focus ion beam deposited carbon-platinum thermometers has been filed under provisional number 63/015,001.

Acknowledgements

This work was performed, in part, at the Center for Integrated Nanotechnologies, an Office of Science User Facility operated for the U.S. Department of Energy (DOE) Office of Science by Los Alamos National Laboratory (Contract DE-AC52-06NA25396) and Sandia National Laboratories (Contract DE-NA-0003525). Sandia National Laboratories is a multimission laboratory managed and operated by National Technology Engineering Solutions of Sandia, LLC, a wholly owned subsidiary of Honeywell International Inc., for the U.S. Department of Energy's National Nuclear Security Administration under contract DE-NA0003525. This work is supported by NSF grant DMR 1807583 and Colorado School of Mines start-up funding. This paper describes objective technical results and analysis. Any subjective views or opinions that might be expressed in the paper do not necessarily represent the views of the U.S. Department of Energy or the United States Government.

References

[1] J.P. Pekola, Towards quantum thermodynamics in electronic circuits, Nat. Phys. 11 (2) (2015) 118–123.
[2] L. Hicks, M.S. Dresselhaus, Effect of quantum-well structures on the thermoelectric figure of merit, Phys. Rev. B 47 (19) (1993) 12727.
[3] T. Harman, P. Taylor, M. Walsh, B. LaForge, Quantum dot superlattice thermoelectric materials and devices, Science 297 (5590) (2002) 2229–2232.
[4] S. Vinjanampathy, J. Anders, Quantum thermodynamics, Contemp. Phys. 57 (4) (2016) 545–579.
[5] F. Giazotto, M.J. Martínez-Pérez, The josephson heat interferometer, Nature 492 (7429) (2012) 401–405.
[6] H. Quan, P. Zhang, C. Sun, Quantum heat engine with multilevel quantum systems, Phys. Rev. 72 (5) (2005), 056110.
[7] J. Millen, A. Xuereb, Perspective on quantum thermodynamics, New J. Phys. 18 (1) (2016), 011002.

[1] Lakeshore, Cernox® Specifications, 2020.

[8] I. Bat'ko, M. Somora, D. Vanickỳ, K. Flachbart, Ruo2-based thick-film resistors as high sensitivity thermometers for millikelvin temperatures, Cryogenics 32 (12) (1992) 1167–1168.
[9] M. Watanabe, M. Morishita, Y. Ootuka, Magnetoresistance of ruo2-based resistance thermometers below 0.3 k, Cryogenics 41 (3) (2001) 143–148.
[10] T. Yotsuya, Y. Kakehi, T. Ishida, Thin film temperature sensor for cryogenic region with small magnetoresistance, Cryogenics 51 (9) (2011) 546–549.
[11] T. Yotsuya, M. Yoshitake, J. Yamamoto, New type cryogenic thermometer using sputtered zr-n films, Appl. Phys. Lett. 51 (4) (1987) 235–237.
[12] V. Mitin, P. McDonald, F. Pavese, N. Boltovets, V. Kholevchuk, I.Y. Nemish, V. Basanets, V. Dugaev, P. Sorokin, R. Konakova, et al., Ge-on-gaas film resistance thermometers for cryogenic applications, Cryogenics 47 (9–10) (2007) 474–482.
[13] N. Boltovets, V. Kholevchuk, R. Konakova, V. Mitin, E. Venger, Ge-film resistance and si-based diode temperature microsensors for cryogenic applications, Sensor Actuator Phys. 92 (1–3) (2001) 191–196.
[14] O. Bourgeois, T. Fournier, J. Chaussy, Measurement of the Thermal Conductance of Silicon Nanowires at Low Temperature, 2007.
[15] J. Heron, T. Fournier, N. Mingo, O. Bourgeois, Mesoscopic size effects on the thermal conductance of silicon nanowire, Nano Lett. 9 (5) (2009) 1861–1865.
[16] T. Nguyen, A. Tavakoli, S. Triqueneaux, R. Swami, A. Ruhtinas, J. Gradel, P. Garcia-Campos, K. Hasselbach, A. Frydman, B. Piot, et al., Niobium nitride thin films for very low temperature resistive thermometry, J. Low Temp. Phys. 197 (5–6) (2019) 348–356.
[17] E. Griffin, J. Mochel, Low temperature, thin film nicr thermometers, Rev. Sci. Instrum. 45 (10) (1974) 1265–1267.
[18] S. Obukhov, New type of cryogenic semiconductor resistance thermometer, Cryogenics 34 (3) (1994) 237–240.
[19] A. Boukai, K. Xu, J.R. Heath, Size-dependent transport and thermoelectric properties of individual polycrystalline bismuth nanowires, Adv. Mater. 18 (7) (2006) 864–869.
[20] M. Singh, J. Wang, M. Tian, T.E. Mallouk, M.H. Chan, Antiproximity effect in aluminum nanowires with no applied magnetic field, Phys. Rev. B 83 (22) (2011) 220506.
[21] A. Fernández-Pacheco, J. De Teresa, R. Córdoba, M. Ibarra, Metal-insulator transition in pt-c nanowires grown by focused-ion-beam-induced deposition, Phys. Rev. B 79 (17) (2009) 174204.
[22] R. Langford, T.-X. Wang, D. Ozkaya, Reducing the resistivity of electron and ion beam assisted deposited pt, Microelectron. Eng. 84 (5–8) (2007) 784–788.
[23] T. Tao, J. Ro, J. Melngailis, Z. Xue, H.D. Kaesz, Focused ion beam induced deposition of platinum, J. Vac. Sci. Technol. B 8 (6) (1990) 1826–1829.
[24] M. Chakravorty, K. Das, A. Raychaudhuri, J. Naik, P. Prewett, Temperature dependent resistivity of platinum–carbon composite nanowires grown by focused ion beam on sio2/si substrate, Microelectron. Eng. 88 (11) (2011) 3360–3364.
[25] J.-F. Lin, J. Bird, L. Rotkina, A. Sergeev, V. Mitin, Large effects due to electron–phonon-impurity interference in the resistivity of pt/c-ga composite nanowires, Appl. Phys. Lett. 84 (19) (2004) 3828–3830.
[26] Y. Tsukatani, N. Yamasaki, K. Murakami, F. Wakaya, M. Takai, Transport properties of pt nanowires fabricated by beam-induced deposition, Jpn. J. Appl. Phys. 44 (7S) (2005) 5683.
[27] L. Penate-Quesada, J. Mitra, P. Dawson, Non-linear electronic transport in pt nanowires deposited by focused ion beam, Nanotechnology 18 (21) (2007) 215203.
[28] J.-F. Lin, J. Bird, L. Rotkina, P. Bennett, Classical and quantum transport in focused-ion-beam-deposited pt nanointerconnects, Appl. Phys. Lett. 82 (5) (2003) 802–804.
[29] K.A. Telari, B. Rogers, H. Fang, L. Shen, R. Weller, D. Braski, Characterization of platinum films deposited by focused ion beam-assisted chemical vapor deposition, J. Vac. Sci. Technol. B 20 (2) (2002) 590–595. Microelectronics and Nanometer Structures Processing, Measurement, and Phenomena.
[30] J. De Teresa, R. Córdoba, A. Fernández-Pacheco, O. Montero, P. Strichovanec, M. Ibarra, Origin of the difference in the resistivity of as-grown focused-ion- and focused-electron-beam-induced pt nanodeposits, J. Nanomater. 2009 (2009) 10.
[31] J. Puretz, L. Swanson, Focused ion beam deposition of pt containing films, J. Vac. Sci. Technol. B 10 (6) (1992) 2695–2698. Microelectronics and Nanometer Structures Processing, Measurement, and Phenomena.
[32] F. Pobell, Matter and Methods at Low Temperatures, vol. 2, Springer, 2007.
[33] P. Kim, L. Shi, A. Majumdar, P.L. McEuen, Thermal transport measurements of individual multiwalled nanotubes, Phys. Rev. Lett. 87 (21) (2001) 215502.
[34] A. Mavrokefalos, A.L. Moore, M.T. Pettes, L. Shi, W. Wang, X. Li, Thermoelectric and structural characterizations of individual electrodeposited bismuth telluride nanowires, J. Appl. Phys. 105 (10) (2009) 104318.
[35] D. Li, Y. Wu, P. Kim, L. Shi, P. Yang, A. Majumdar, Thermal conductivity of individual silicon nanowires, Appl. Phys. Lett. 83 (14) (2003) 2934–2936.
[36] L. Shi, D. Li, C. Yu, W. Jang, D. Kim, Z. Yao, P. Kim, A. Majumdar, Measuring thermal and thermoelectric properties of one-dimensional nanostructures using a microfabricated device, J. Heat Tran. 125 (5) (2003) 881–888.
[37] F. Zhou, J. Szczech, M.T. Pettes, A.L. Moore, S. Jin, L. Shi, Determination of transport properties in chromium disilicide nanowires via combined thermoelectric and structural characterizations, Nano Lett. 7 (6) (2007) 1649–1654.
[38] W. Black Jr., W. Roach, J. Wheatley, Speer carbon resistors as thermometers for use below 1 k, Rev. Sci. Instrum. 35 (5) (1964) 587–591.
[39] J. Clement, E. Quinnell, The low temperature characteristics of carbon-composition thermometers, Rev. Sci. Instrum. 23 (5) (1952) 213–216.
[40] I. Beloborodov, A. Lopatin, V. Vinokur, K. Efetov, Granular electronic systems, Rev. Mod. Phys. 79 (2) (2007) 469.
[41] S. Kirkpatrick, Percolation and conduction, Rev. Mod. Phys. 45 (4) (1973) 574.
[42] W. Cai, H. Zhong, L. Zhang, Optical measurements of oxidation behavior of silver nanometer particle within pores of silica host, J. Appl. Phys. 83 (3) (1998).
[43] D.N. McIlroy, D. Zhang, M. Grant Norton, W.L. O'Brien, M.M. Schwickert, G.R. Harp, Synthesis and reactivity of fe nanoparticles embedded in a semi-insulating matrix, J. Appl. Phys. 87 (10) (2020).
[44] H. Yoshida, H. Omote, S. Takeda, Oxidation and reduction processes of platinum nanoparticles observed at the atomic scale by environmental transmission electron microscopy, Nanoscale 6 (21) (2014) 13113–13118.
[45] G.D. Marzi, D. Iacopino, A.J. Quinn, G. Redmond, Probing intrinsic transport properties of single metal nanowires: direct-write contact formation using a focused ion beam, J. Appl. Phys. 96 (6) (2004) 3458–3462.
[46] A. Bid, A. Bora, A. Raychaudhuri, Temperature dependence of the resistance of metallic nanowires of diameter 15 nm: applicability of bloch-grüneisen theorem, Phys. Rev. B 74 (3) (2006), 035426.